JOURNAL OF
Materials
CHEMISTRY

Preparation, characterization and thermal evolution of oxygen passivated nanocrystalline cobalt

Teresa C. Rojas, Juán C. Sánchez-López, María J. Sayagués, Ettireddy P. Reddy, Alfonso Caballero and Asuncion Fernández*

Instituto de Ciencia de Materiales de Sevilla and Dpto. de Química Inorgánica, Centro de Investigaciones Científicas Isla de la Cartuja, Avda. Américo Vespucio s/n, 41092–Sevilla, Spain. E-mail: asuncion@cica.es

Received 19th October 1998, Accepted 5th February 1999

Nanocrystalline cobalt powders have been prepared by the inert gas evaporation method. After preparation the materials were passivated by pure oxygen and air exposure. In the present paper we describe the application of different techniques like transmission electron microscopy (TEM), X-ray diffraction (XRD), X-ray photoelectron spectroscopy (XPS), X-ray absorption spectroscopy (XAS) and electron energy loss spectroscopy (EELS) to achieve an exhaustive chemical and structural characterization of the nanocomposite material in its original state (passivated Co powder) and after thermal treatments in vacuum. After passivation the cobalt fcc nanocrystals (typical sizes 2–20 nm) are covered by an amorphous oxide passivation layer with a short range structural order similar to the cubic (fcc) CoO phase. Upon heating, crystallisation of the oxide layer is observed together with the formation of the Co_3O_4 spinel phase. *In situ* XPS experiments allow the determination of the relative amounts of oxide and metal as a function of the oxygen dose. The present study is relevant due to the correlation between microstructure and the unusual magnetic properties of this type of material.

Introduction

Research in the field of fine magnetic particles has been very active in the last few decades due to their potential applications in many areas of technology including high density magnetic recording media.[1–3] Their small size (1 to a few tens of nm) not only makes them better recording media due to their superior magnetic properties, but also opens up an interesting scientific problem on finite size effects. A number of research works have been published during the last few years dealing with the magnetic behaviour of nanometric Fe, Co and Ni nanocrystalline particles presenting different degrees of surface oxidation.[4–12] The singular magnetic behaviour of these systems has been found to be dependent on the size and the surface characteristics of the particles, and it is attributed to the large magnetic anisotropies observed in these materials. In particular, exchange anisotropy was first discovered by Meiklejohn and Bean[10] in compacted oxide-coated Co particles. In spite of the numerous publications on the magnetic properties of oxide coated Fe, Co and Ni nanoparticles, there is still a limited number of studies on the characterization of these systems at the microstructural level to achieve a better understanding of the properties.[13,14]

In the present paper we describe the use of many different techniques to characterize Co nanocrystalline particles coated with an oxide layer: transmission electron microscopy (TEM), X-ray diffraction (XRD), X-ray photoelectron spectroscopy (XPS), X-ray absorption spectroscopy (XAS) and electron energy loss spectroscopy (EELS). The nanocrystalline Co powders have been prepared by the inert gas evaporation method.[15] After passivation by pure oxygen and air exposure the final Co-oxide/Co nanocomposite was obtained. Conclusions about the chemical composition and local structure of the nanocomposite material are related to the effect of exchange anisotropy in nano-sized oxide-metal coupled systems.

Experimental

The experimental device used for the synthesis of the Co ultrafine grains consists of a small HV chamber pumped to a residual vacuum better than 5×10^{-7} Torr. A tungsten boat containing a pressed pellet of Co powder (from Goodfellow Metals, 99.9% pure) was heated resistively to a temperature of *ca.* 1773 K in a He atmosphere of 1 Torr. The evaporated material loses kinetic energy by collisions with the inert gas atoms and condenses as small particles that were collected on a cold substrate.[15] After preparation, the powder was passivated by oxygen (3 Torr for 10 min) before exposure to air. The loose material was collected (smoothly stripped off) from two regions: one in direct contact with a liquid nitrogen reservoir located at a large distance from the evaporation source and a second one situated at a shorter distance from the evaporation device. Two portions of the sample were separated and named hereafter as Co-oxide/Co(A) and Co-oxide/Co(B), respectively.

It has been experimentally stated that both samples show a shift of the field cooled hysteresis loop. This behaviour corresponds to the exchange interaction of the oxide layer with the ferromagnetic core, typically observed in these type of samples[9,10] and will be the object of further work.

TEM examination of the samples was carried out in a Philips CM200 microscope working at 200 kV. The samples were dispersed in ethanol by sonication and dropped on a copper grid coated with a carbon film. Dark field mode was used by tilting the incident illumination to bring the (200) diffraction ring for metallic cobalt into the position of the central spot.

The intensities of the electron diffraction rings from the polycrystalline samples were integrated using the FIT2D program[16] leading to plots of diffraction intensity against the θ angle.

High resolution TEM images were obtained in a JEOL 4000 EX(II), operating at 400 kV with a LaB_6 filament. The instrument is equipped with a top entry goniometer (±20° tilt specimen holder). The point resolution in this microscope is about 0.16 nm.

XRD analysis was carried out using Cu Kα radiation in a Siemens D5000 diffractometer.

XPS spectra were recorded in a VG-Escalab 210 spectrometer working in the constant analyser energy mode with a pass energy of 50 eV and using Mg-Kα radiation as the excitation source. The binding energy (BE) reference was taken at the C 1s peak from carbon contamination of the samples at 284.6 eV. An estimated error of ±0.1 eV can be assumed for all measurements. For the *in situ* XPS analysis the Co nanoparticles were prepared in the pretreatment chamber of our spectrometer in which we included the same evaporation system as used in the *ex situ* preparation chamber. The nanocrystalline material, deposited on a tantalum foil situated in the spectrometer sample holder, was examined by XPS directly after transfer to the analysis chamber. The samples were also analysed after the *in situ* exposure to a controlled oxygen atmosphere pressure.

XAS spectra were recorded at the DCI storage ring in LURE (France), running at 1.85 GeV with an average current of 250 mA. Monochromatisation of the beam was carried out through a Si(111) double crystal monochromator. The detection of the XAS absorption coefficient was done in the transmission mode for the samples that were supported on cellulose filters. Spectra were recorded at the Co K edge at *ca.* 7720 eV. To compare the XAS spectra a linear background was fitted in the pre-edge region and subtracted before normalisation to the edge jump.

EELS spectra were acquired in the Philips CM200 microscope operating at 200 kV and equipped with a Gatan model 766–2K parallel detection electron spectrometer. In order to record the O K-edge and Co $L_{2,3}$-edges the illuminated area was *ca.* 1 μm in diameter. Spectra were recorded in the diffraction mode with a camera length of 700 mm and a collection angle of *ca.* 1 mrad. An EELS entrance aperture of 3 mm was also used. The measured energy resolution at the zero-loss peak of the coupled microscope/spectrometer system was about 3 eV. Spectra were recorded for dark current and channel-to-channel gain variation. A low-loss spectrum was also recorded with each edge in the same illuminated area. After subtraction of the background with a standard power-law function, the spectra were deconvoluted for plural scattering with the Fourier-ratio method. All these treatments were performed within the EL/P program (Gatan).

Results and discussion

In Fig. 1 we have included TEM micrographs for samples Co-oxide/Co(A) (top) and Co-oxide/Co(B) (bottom). The samples appear to be formed from almost spherical grains forming agglomerates and also showing a high degree of coalescence or interconnection between grains. The nanometric character of the samples is clear showing particle sizes of around 9–20 nm for sample A and 9–30 nm for sample B.

The XRD diffractograms of the passivated nanocrystalline samples (Fig. 2 left) indicate the presence of metallic cobalt in the fcc phase. It is interesting to mention that the starting Co powder material for evaporation was hexagonal cobalt. Similar behaviour has been reported for erbium[17] and yttrium oxides[18] where high-pressure polymorphic phases can be stabilized in grains of a few nanometers in diameter. The peaks in Fig. 2 (left) are very broad, especially in sample Co-oxide/Co(A) indicating the very small crystallite size of the metallic phase. The cobalt oxide passivation layer should be quite amorphous or very thin and consequently no clear peaks from CoO or Co_3O_4 phases could be identified. Other techniques may then be used to obtain more information on the structure of this amorphous oxide layer.

In this sense, in addition to a bulk analysis technique like XRD, we have used a surface sensitive technique like XPS. The Co 2p photoelectron spectra of both samples are depicted in Fig. 2 (right). The spectra show four main peaks, the doublet $2p_{3/2}$ and $2p_{1/2}$ and the shake-up resonance transitions of these two peaks at higher binding energies. The position of the main doublet is compared with the energies of the corresponding photoelectrons in metallic cobalt, CoO and Co_3O_4. The literature values[19] for the $2p_{3/2}$ peak in Co^0 is *ca.* 778.1 eV while for the cobalt oxide phases the corresponding value is around 780.2 eV. The comparison with the values depicted in Fig. 2 (right) for the samples under investigation (780.5 and 781.5 eV for samples B and A respectively) indicates clearly that the surface of the particles is fully oxidised. The displacement of the peaks to higher binding energies, in respect to the ones reported for the CoO and Co_3O_4 references, may be attributed to the presence of $Co(OH)_2$ species[20] formed by water adsorption on the surface of ultrafine powders. In addition, the high intensity of the shake-up satellites at *ca.* 786 and 802 eV is characteristic of Co(II) species[21] while Co(III) states show a strong decrease in the intensity of these satellites.[22] The absence of metallic cobalt in the XPS analysis

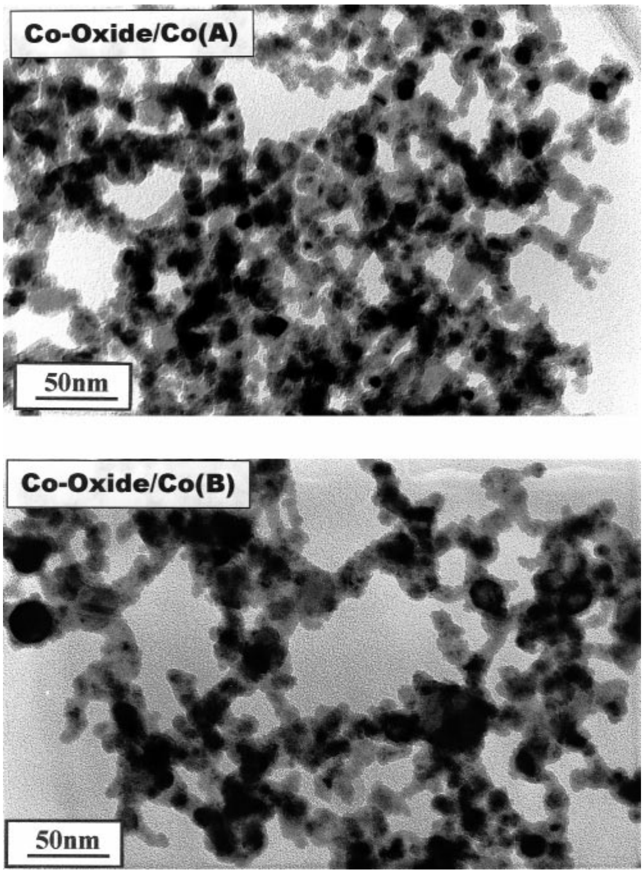

Fig. 1 TEM bright field micrographs for Co-oxide/Co(A) (top) and Co-oxide/Co(B) (bottom) samples.

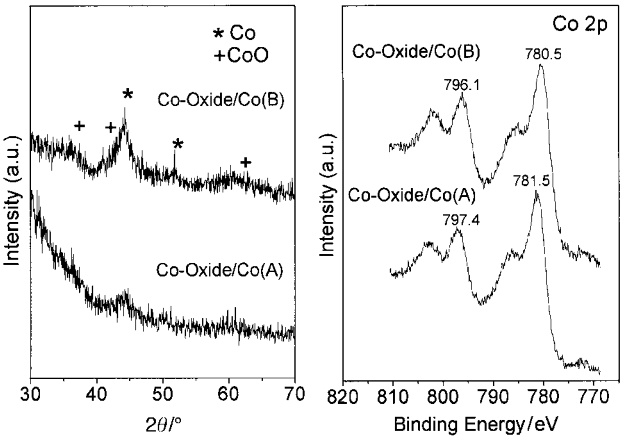

Fig. 2 XRD diffraction patterns (left) and Co 2p photoelectron spectra (right) for the Co-oxide/Co(A) and (B) samples.

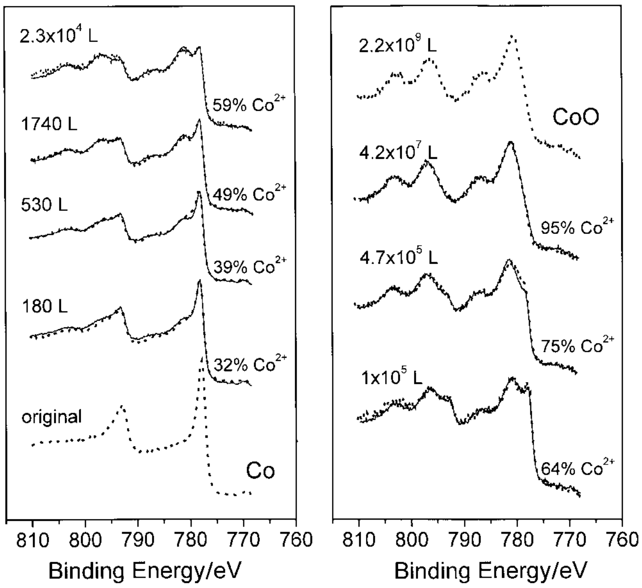

Fig. 3 Co 2p photoelectron spectra of the *in situ* prepared nanocrystalline cobalt (original) and after exposure to different doses of oxygen. The experimental spectra are depicted as dotted line. Full lines correspond to the best fitted linear combination of the spectra for pure Co and CoO phases.

indicates that the passivation oxide layer is thicker than *ca.* 3 nm, the penetration depth of the photoelectron analysis. It is also worth mentioning that this technique gives important information related to the major presence of Co^{2+} species, indicating the formation of a CoO like oxide layer after room temperature passivation of the nanocrystalline Co particles.

To characterise the formation of the oxide layer on the Co particles, we performed an *in situ* XPS study of the oxygen passivation process of metallic cobalt nanoparticles. XPS was then used to follow the evolution of the Co 2p photoelectron peaks as a function of the oxygen dose (see Fig. 3). The spectra change from the pure metallic cobalt to the pure oxide phase. By linear combination of these two extreme spectra we could quantify the degree of surface oxidation as a function of the oxygen dose. In Fig. 3 we show these linear combinations and how they fit to the experimental data. The results are depicted in Fig. 4 where we show the percentage of oxidation, as detected by XPS, is represented as a function of the oxygen dose. It was observed that an appreciable oxidation of the nanoparticles occurs just by exposure of the sample to 30 Langmuirs of oxygen (1 Langmuir $= 10^{-6}$ Torr during 1 s). The oxidation then progresses very rapidly to generate a steady state situation by exposure to 4.2×10^7 Langmuirs of oxygen. This situation may correspond to a lower limit of the thickness expected for the oxide layer according to the probing depth of the XPS technique (*ca.* 3 nm).

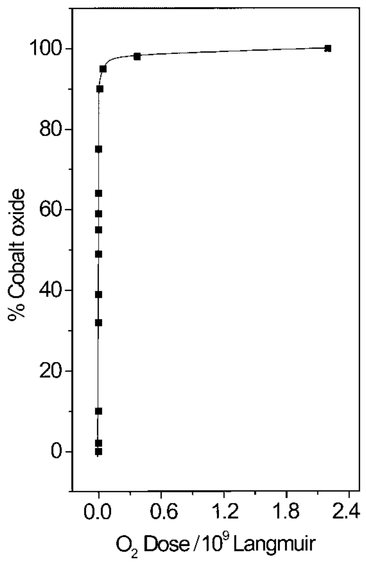

Fig. 4 Percentage of oxidised cobalt in the total Co 2p photoelectron peak as a function of the oxygen dose during the *in situ* oxidation of the nanocrystalline cobalt.

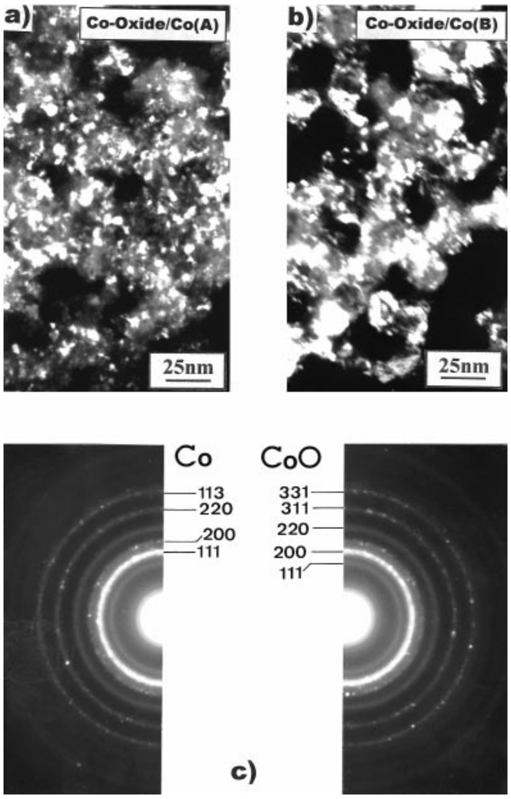

Fig. 5 (a) and (b) TEM dark field images (200 plane for Co^0) as obtained for Co-oxide/Co(A) and Co-Oxide/Co(B) samples. (c) Indexed electron diffraction pattern from the as prepared Co-oxide/Co samples.

A typical electron diffraction pattern obtained for the samples is included in Fig. 5 (bottom). The rings can be indexed according to metallic cobalt and cubic CoO phases. The oxide phase may crystallise partially under the electron beam but it is interesting that in agreement with the XPS results the initially formed oxide phase corresponds to CoO. The rings for the metallic Co phase show some defined diffraction spots indicating the presence of well formed crystallites. In the case of the oxide phase, the diffraction rings are more continuous and diffuse indicating the formation of very small nanocrystals. Furthermore we will show later in this work how controlled electron beam heating can induce transformations in the samples.

Dark field images allow one to distinguish different phases so that by selecting the (200) ring for metallic cobalt the resulting image highlights the cobalt nanocrystals. It is clearly observed in Fig. 5 (top) that sample Co-oxide/Co(A) contains smaller Co crystallites than sample Co-oxide/Co(B). Typical crystallite sizes for metallic cobalt of 2–10 and 2–20 nm were measured for samples A and B, respectively. This result is also in good agreement with the XRD pattern in Fig. 2. For samples of crystallite sizes of a few nanometers, the high resolution transmission electron microscopy technique can provide more reliable information than the XRD technique. Fig. 6 presents a high resolution image of the Co-oxide/Co(A) sample showing small metallic Co crystallites embedded in an oxide layer. As can be deduced from this figure crystallisation of the cobalt oxide layer can occur under the high energy

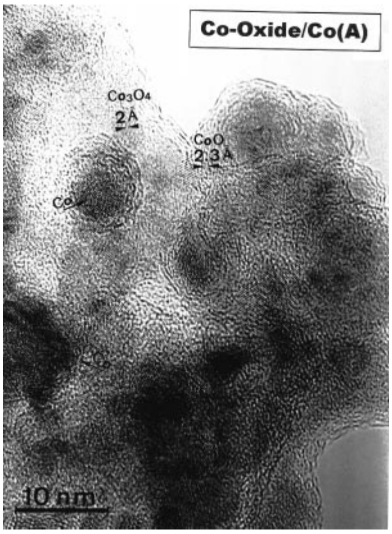

Fig. 6 High resolution TEM image for the Co-oxide/Co(A) sample.

(400 kV) electron beam as we will describe below. Consequently CoO and even Co_3O_4 small crystals can be identified (marked) in this micrograph.

None of the above described analysis techniques could provide a quantitative estimation of the metal/oxide ratio in these samples. The XANES (X-ray absorption near edge structure) region of the XAS spectra contains information about oxidation states and local structure around the absorbing atom. Although multiple scattering calculations can be carried out to simulate the XANES spectra, a fingerprint technique can also be used to obtain conclusions from these data just by comparison with reference samples.[23] In this sense we have plotted in Fig. 7 (left) and 8 (left) the spectra at the Co K-edge for samples Co-oxide/Co(A) and Co-oxide/Co(B) respectively. These spectra are compared to the ones from a metallic Co foil and a CoO reference sample. The first region in the spectra corresponds to a low energy shoulder before the edge threshold at *ca.* 7713 eV. This shoulder is usually attributed to the 1s→3d transition which in perfect O_h symmetry is strictly dipole-forbidden. However, due to the mixing of p- and d-like states this feature is visible. While the energy position of this transition is found to be not very sensitive to the oxidation state and local structure, the intensity of the peak is strongly dependent on them as demonstrated in Fig. 7 (left) and 8 (left) for the Co^0 and CoO references. The second region of the spectra corresponds to the sharp rise for the excitation of the 1s electron into the ionization continuum. In the third region a few eV above the threshold, the final states of the photoelectron should be described as unoccupied bands close to the Fermi level. Because of the fully screened core hole, the near edge spectrum probes the ground-state unoccupied local density of states of the material. In this sense the strong absorption at about 7727 eV can be assigned to the 1s→4p transition and is clearly dependent on the oxidation state of the metal. We should also take into consideration the mixing of 4s, 4p and 3d orbitals.

Just by comparison of the Co K edge spectra for samples A and B with the reference spectra in Fig. 7 (left) and 8 (left), we observe a higher intensity of the features at 7713 and 7760 eV and a decrease in the intensity of the peak at 7727 eV for sample B in comparison to sample A. This corresponds to a higher content of metallic Co in sample B. To quantify the oxide to metal ratio, linear combinations of the reference spectra for Co^0 and CoO have been carried out to achieve the best reproduction of the experimental spectrum for both samples. These linear combinations for samples Co-oxide/Co(A) and Co-oxide/Co(B) are represented in Fig. 7 (right) and 8 (right) giving a quantification of the bulk composition of the oxide–metal nanocomposite materials. The best matched spectra for both samples were found for a composition of 40 and 20% of metalic cobalt in samples A and B respectively. It should be considered here that better reproduction of the experimental spectra should be obtained if we could use a reference spectrum for amorphous CoO instead of the one for a microcrystalline sample. The possibility of using XANES spectroscopy to give a quantification of the oxide to metal atomic ratio is an important advantage of this technique within the characterisation we are presenting in this work.

In an analogous way to that described for XAS, electron energy loss spectroscopy (EELS) is another technique available for the characterisation of nanostructured powders by recording core level absorption edges. The EELS technique in a transmission electron microscope can provide information at a microscopic level while XAS is obtained as an average of the macroscopic sample. In fact, provided that the collection angle of the spectrometer is small (to be consistent with the dipole approximation), it has been shown that EELS can be expressed with the same formalism as the well known XAS.[24] The advantage of EELS over XAS is that the analysed volume can be several orders of magnitude lower, since the electron interaction is strong compared to that of photons. The EELS is limited, however, to elements of lower Z for which the K or L edges are attainable. Also the electron-loss near-edge structure (ELNES) region of the EELS spectra may provide chemical and structural information in a way analogous to

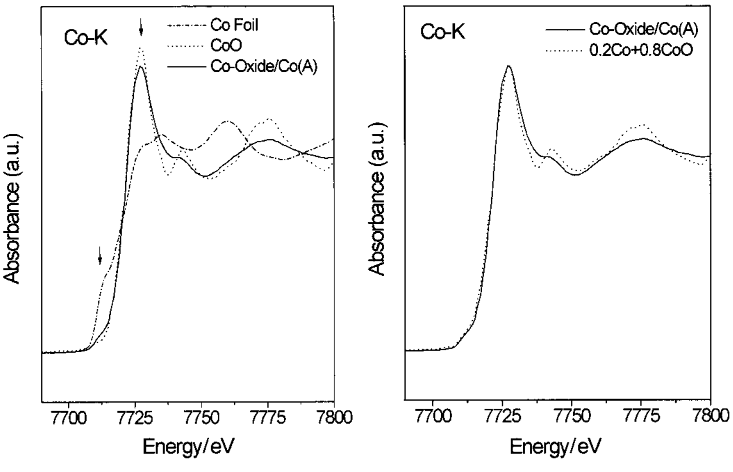

Fig. 7 Left: XAS spectrum at the Co K edge for the Co-oxide/Co(A) sample in comparison to a metallic Co foil and a CoO reference sample. Right: the spectrum for the nanocrystalline composite sample (full line) is compared with the linear combination (dashed line) of the spectra for Co and CoO.

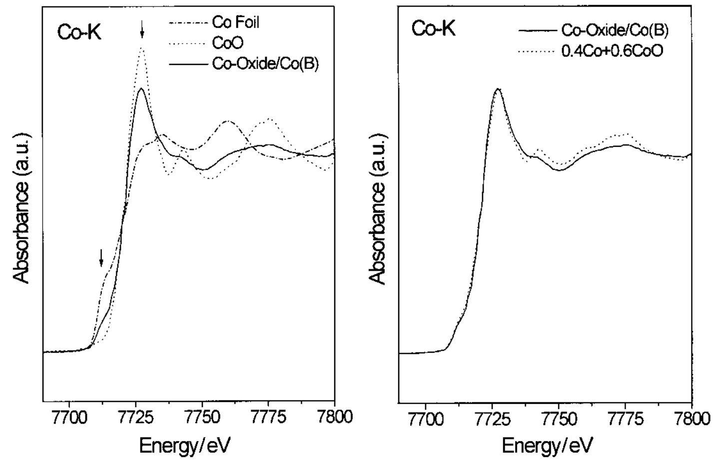

Fig. 8 Left: XAS spectrum at the Co K edge for the Co-oxide/Co(B) sample in comparison to a metallic Co foil and a CoO reference sample. Right: the spectrum for the nanocrystalline composite sample (full line) is compared with the linear combination (dashed line) of the spectra for Co and CoO.

the X-ray absorption near-edge structure (XANES) region of the XAS spectra. In the present work the O K-edge and Co $L_{2,3}$-edges were recorded for the two samples under investigation by EELS at the transmission electron microscope.

In Fig. 9 the EELS spectra of two different regions of sample Co-oxide/Co(A) are shown. It is clear how at the microscopic level the sample is heterogeneous showing zones with different proportions of oxide to metal. This illustrates the fact that XAS is giving us an average of the total sample while EELS can be resolved at the microscopic level. The spectra in this figure are normalised to the jump at the Co $L_{2,3}$ edge. The area at the top has a higher amount of oxide, corresponding to a more intense oxygen K-edge peak. At the Co $L_{2,3}$ edge contributions from both metallic and oxidised cobalt may be present. It is well known that the intensities of Co L_3 and L_2 edge resonances, corresponding to 2p→3d transitions, reflects the occurrence of vacancies in the d band.[25,26] For this reason, the intensities of the resonances increase in Fig. 9 for the region with a higher content of oxidised cobalt (higher density of vacancies at the d band) in comparison to the spectrum obtained from the region with a higher content of metallic cobalt.

During recording of the EELS spectra we realised that the sample could evolve by heating under the electron beam. This provides the possibility of following *in situ* the thermal evolution in vacuum of the samples in the transmission electron microscope. In Fig. 10 we show the O K-edge and Co $L_{2,3}$-edges for the as-prepared Co-oxide/Co(A) sample and the same region after electron beam heating. The spectrum for metallic Co is also included for comparison. The spectra in this figure are normalised to the jump at the Co $L_{2,3}$ edge. Important changes are observed, especially at the O K edge. With respect to the Co $L_{2,3}$ edges, it is clear that the differences in the intensity of the edge resonances between a metallic Co foil and our samples may be attributed to the presence of an oxide passivation layer.

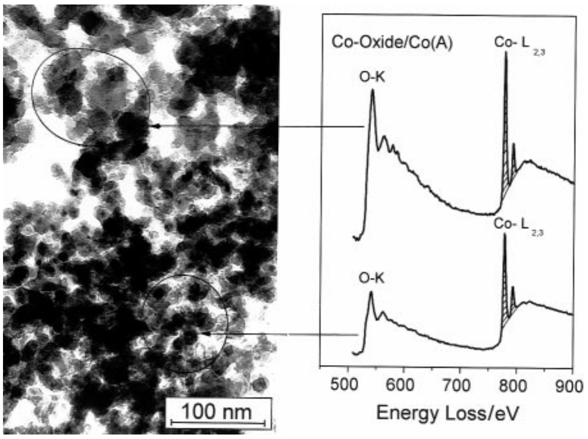

Fig. 9 Left: TEM micrograph of the Co-oxide/Co(A) sample. Right: EELS spectra at the O K-edge and Co $L_{2,3}$-edges for two different zones of the same sample. The areas of the edge resonances have been shaded.

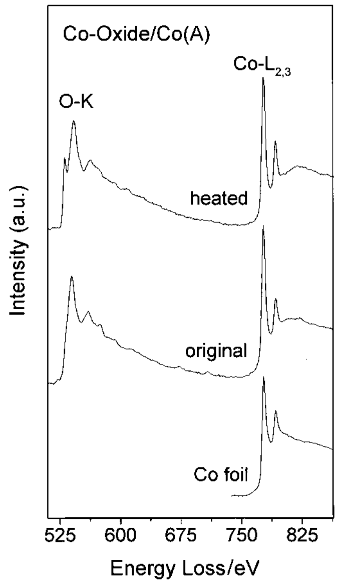

Fig. 10 O K-edge and Co $L_{2,3}$-edges for the Co-oxide/Co(A) sample in its original state and after heating under vacuum under electron beam illumination. The spectrum for a metallic Co reference sample has also been included.

Fig. 11 shows the evolution of the O K-edge of the Co-oxide/Co(A) sample from its original state under heating by electron beam irradiation. The spectra have been normalised to the height of the peak at 543 eV and aligned to the position of the main peak also at 543 eV in order to allow easy comparison of the spectra. The original sample shows a short range local order similar to that of the CoO phase. However, the peaks appear broader, corresponding to an amorphous CoO phase. The position of the shoulder in the original sample at *ca.* 534 eV corresponds to the well defined peak in the CoO reference. Upon heating by electron beam illumination we observe initially a crystallisation of the CoO phase as indicated by the resolution of the broad features. However, the O K-

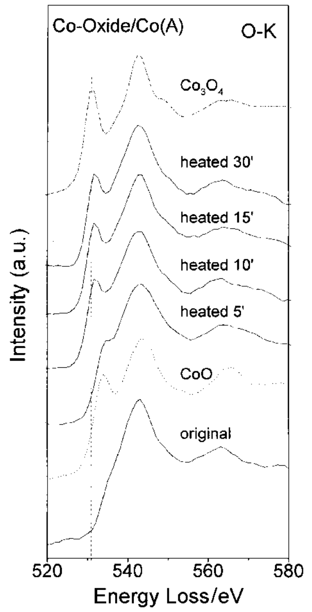

Fig. 11 Evolution of the O K edge, as recorded by EELS, for the Co-oxide/Co(A) sample from its original state under electron beam illumination. For comparison spectra for CoO and Co_3O_4 reference samples are included.

edge spectra evolve very soon to the formation of a Co_3O_4 phase as indicated by the shift of the band position to 531 eV and the increase of the intensity of the first peak in the spectrum. This transition, just above the edge jump, is assigned to the 1s→2p excitation and reflects the partial density of O 2p unoccupied electronic states. In addition these states are also hybridized with the minority e_g states so that this feature is in agreement with the structure of cobalt oxide and a fingerprint method has again been used here to obtain information on the structure of the nanocrystalline materials.

It should be mentioned here that the resolution of the EELS or XAS data can be improved, depending on the available experimental facilities, leading to better resolved spectra.

The thermal evolution of the samples can also be followed by electron diffraction. The integration of the diffraction rings leads to the curves presented in Fig. 12 as a function of the diffraction angle. It is possible to identify peaks corresponding to metallic fcc Co, cubic CoO and Co_3O_4 spinel phases. The original samples contain metallic Co and a CoO like overlayer. This oxide passivation layer evolves to a Co_3O_4 crystalline phase in good agreement with the previously described EELS results.

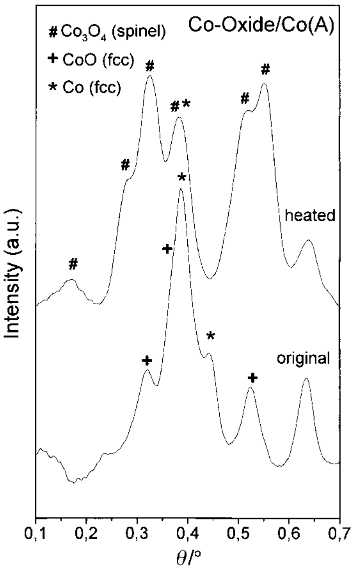

Fig. 12 Integrated electron diffraction pattern for the original Co-oxide/Co(A) sample and after heating in vacuum under electron beam illumination. Expected θ angles for the rings corresponding to Co (fcc), CoO (fcc) and Co_3O_4 spinel phases are included.

Conclusions

Several conclusions can be derived from the above described analysis.

(i) A combination of complementary techniques has been demonstrated to be necessary to achieve a complete chemical and structural analysis of nanostructured ultrafine powders. In particular, oxygen passivated nanocrystalline cobalt has been studied.

(ii) The XRD technique shows limitations for the structural analysis of very small crystallites and for characterization of nanoscopic amorphous passivation layers.

(iii) XPS, as a surface analysis technique, can give us information about the oxidation state of the metal in the oxide passivation layer. However, it cannot give a quantification of the relative amount of metal and oxide in the final passivated sample. By following *in situ* by XPS the oxidation of cobalt metallic nanoparticles, we found that a dose of just 30 Langmuirs produces appreciable oxidation of the surface of the cobalt nanoparticles. With doses of *ca.* 4.2×10^7 Langmuirs a thickness of the oxide layer of approximately 3 nm is already produced.

(iv) XAS appears to be a useful tool to quantify the amount of metal and oxide present in the samples. We found compositions of 40 and 20% metallic cobalt in samples A and B respectively. It should be emphasized that the amount of oxide present in this type of sample is higher than normally assumed.

(v) EELS appears similar to XAS but it has the advantage of the lateral resolution obtained in the microscope. The energy resolution is not as good as in XAS but we can identify different regions at the microscopic level.

(vi) TEM studies show that the metallic cores are always covered by the oxide passivation layer. In some regions the cobalt nanocrystals even appear to be embedded in an oxide matrix. This feature is different from the normally assumed core shell structure where a very thin oxide layer is expected to cover the metallic particles.

(vii) The nanoscopic structure of the materials explains their known magnetic behaviour.[10,11] A high degree of interaction between the ferromagnetic (metallic core) and the antiferromagnetic (or ferrimagnetic) oxide phases is expected from this microstructural study. It should be also emphasized that the oxide passivation layer is initially amorphous, and this may also be considered when attempting to understand the spin glass like behaviour of this type of sample.[11]

(viii) Finally it is interesting to mention the stabilization of the cubic Co phase in the nanocrystals and also the stabilization of the Co_3O_4 phase in the oxide layer upon heating. The nanometric character of these systems leads to the stabilization of certain phases, in some cases metastable phases, as a consequence of the nanometric character of the samples.[17,18,27]

Acknowledgements

The authors thank the DGES for financial support (Project no. PB96–0863-C02–02). The Department of Materials (Oxford University) and the synchrotron LURE are acknowledged for providing the HRTEM and XAS facilities. EC COST Action 523 ‘Nanostructured Materials’ is also gratefully acknowledged.

References

1 E. Matijevic, *MRS Bull.*, 1989, Vol. XIV, 19.

2 Y. Yoshizawa, S. Oguma and K. Yamauchi, *J. Appl. Phys.*, 1988, **64**, 6044.

3 E. F. Kneller and R. Hawig, *IEEE Trans. Magn. MAG-27*, 1991, 3588.

4 W. Wagner, H. Van Swygenhoven, H. J. Höfler and A. Wiedenmann, *Nanostruct. Mater.*, 1995, **6**, 929.

5 W. Gong, H. Li, Z. Zhao and J. Chen, *J. Appl. Phys.*, 1991, **69**, 5119.

6 S. Gangopadhyay, G. C. Hadjipanayis, S. I. Shah, C. M. Sorensen, K. J. Klabunde, V. Papaefthymiou and A. Kostikas, *J. Appl. Phys.*, 1991, **70**, 5888.

7 J. Löffler, H. Van Swygenhoven, W. Wagner, J. Meier, B. Doudin and J.-Ph. Ansermet, *Nanostruct. Mater.*, 1997, **9**, 523.

8 H. Kisker, T. Gessmann, R. Würschum, H. Kronmüller and H. E. Schaefer, *Nanostruct. Mater.*, 1995, **6**, 925.

9 S. Gangopadhyay, G. C. Hadjipanayis, B. Dale, C. M. Sorensen and K. J. Klabunde, *Nanostruct. Mater.*, 1992, **1**, 77.

10 W. H. Meiklejohn and C. P. Bean, *Phys. Rev.*, 1957, **105**, 904.

11 L. del Bianco, A. Hernando, M. Multigner, C. Prados, J. C. Sánchez-López, A. Fernández, C. F. Conde and A. Conde, *J. Appl. Phys.*, 1998, **84**, 2189.

12 S. Gangopadhyay, G. C. Hadjipanayis, B. Dale, C. M. Sorensen, K. J. Klabunde, V. Papaefthymiou and A. Kostikas, *Phys. Rev. B*, 1992, **45**, 9778.

13 T. Uchikoshi, Y. Sakka, M. Yoshitake and K. Yoshihara, *Nanostruct. Mater.*, 1994, **4**, 199.

14 J. Löffler, W. Wagner, H. Van Swygenhoven and A. Wiedenmann, *Nanostruct. Mater.*, 1997, **9**, 331.

15 H. Gleiter, *Adv.Mater.*, 1992, **4**, 474.

16 The authors thank Dr. A. P. Hammersley and the European Synchrotron Radiation Facility (ESRF) for allowing us the use of the FIT2D program for analysis of two dimensional images.

17 Z. Li, H. Hahn and R. Siegel, *Mater. Lett.*, 1988, **6**, 342.

18 G. Skandan, C. M. Foster, H. Frase, M. N. Ali, J. C. Parker and H. Hahn, *Nanostruct. Mater.*, 1992, **1**, 313.

19 *Practical Surface Analysis. Volume 1: Auger and X-Ray Photoelectron Spectrosocpy*, ed. D. Briggs and M. P. Seah, John Wiley, New York, 1990.

20 N. S. McIntyre and M. G. Cook, *Anal. Chem.*, 1975, **47**, 2210.

21 S. Hofmann and J. M. Sanz, *Fresenius' Z. Anal. Chem.*, 1983, **314**, 215.

22 P. S. Ho and J. E. Lewis, *Surf. Sci.*, 1976, **55**, 335.

23 A. Bianconi *X-Ray Absorption: Principles, Applications, Techniques of EXAFS, SEXAFS and XANES*, ed. D. C. Konigsberger and R. Prins, John Wiley, New York, 1988, ch. 11, pp. 573–662.

24 W. L. Schaich, *Phys. Rev. B*, 1984, **29**, 6513.

25 J. A. Horsley, *J. Chem. Phys.*, 1982, **76**, 1451.

26 G. Meitzner, J. H. Sinfelt and D. A. Fischer, *X-Ray Absorption Fine Structure*, ed. S. Samar Hasnain, Ellis Horwood, New York, 1991, ch. 142, p. 533.

27 J. C. Sánchez-López and A. Fernández, *Mater. Sci. Forum*, 1998, **269–272**, 827.

Paper 8/08098D